Response of helium bubbles in gold to displacement-cascade damage

S. E. Donnelly

Joule Laboratory, Science Research Institute, University of Salford, M5 4WT, United Kingdom

R. C. Birtcher

Materials Science Division, Argonne National Laboratory, Argonne, Illinois 60439

C. Templier

Laboratoire de Métallurgie Physique, Université of Poitiers, 40 Avenue du Recteur Pineau, 86022 Poitiers Cédex, France

V. Vishnyakov

Joule Laboratory, Science Research Institute, University of Salford, M5 4WT, United Kingdom

Evolution of He bubbles in Au has been followed with *in situ* electron microscopy during 400 keV Ar ion irradiation at 500 K. He bubbles were produced by implantation at 500 K of 3 keV He ions into prethinned Au samples that were then annealed to 670 K. During Ar irradiation, bubbles undergo athermal migration, coalescence, and disintegration. The bubbles after annealing were underpressurized, but Ar irradiation brought the bubbles to equilibrium pressure after a dose of 0.6 displacements per atom (dpa). Bubble behavior can be understood on the basis of their interactions with adjacent cascades. We propose that a discrete bubble jump is induced by the melt zone formed during the thermal spike phase of a contiguous cascade. The rate of bubble migration is modeled with the assumption that the jump distance is determined by the bubble and cascade volumes.

INTRODUCTION

Inert gases in solids have been studied for the past four decades driven primarily by materials problems associated with the operation of both nuclear fission and fusion reactors.[1] Interest in helium arose because of its relevance to first wall integrity in the proposed fusion reactor and to helium embrittlement in nuclear reactors. In addition, studies of helium in elemental metals can provide insights into fundamental behavior relevant to more complex systems such as heavy inert gases in nuclear fuels. A number of interesting phenomena have been observed for this system. These include small bubbles containing helium at pressures of tens of thousands of atmospheres or greater,[2,3] helium bubble superlattices,[4] and helium platelets.[5] However, a number of general questions remain unanswered regarding inert gases in metals. Of particular importance from a technological viewpoint is the behavior of gas bubbles in the complex environment of a reactor where both high temperatures and damaging irradiation have important influences on bubble kinetics. Although there has been continued interest since the early 1960s in the role of irradiation-induced release of fission gas from nuclear fuels[5–9] scant direct information is available on the behavior of inert gas bubbles under irradiation.

This paper reports observations of the evolution of helium bubbles in a high-Z metal, gold, during irradiation with 400 keV Ar ions. The study utilized an ion irradiation facility *in situ* in a high-voltage electron microscope (HVEM) allowing the detailed behavior of individual bubbles to be followed by transmission electron microscopy (TEM). The behavior observed in the present work differs significantly from that observed previously for a low-Z material, Al, during heavy ion irradiation.[10]

He bubble growth in Al was observed to take place by irradiation induced coalescence of bubbles without bubble motion. Bubbles decreased in size at an average rate of 0.024 to 0.048 nm/dpa (displacements per atom) due to direct displacement of He out of the bubble while the bubble remained at equilibrium pressure. He resolution occurred at a rate of 0.005 to 0.01 He$^{\text{ejected}}$/He/dpa. Bubble centers remained fixed during bubble shrinkage indicating negligible bubble motion during room-temperature irradiation. No examples were found that would indicate complete destruction of a bubble in Al by a single ion.

EXPERIMENT

Specimens were prepared by jet-polishing polycrystalline Au (99.9999 at. % pure) TEM discs with grain size greater than 10 μm. These were subsequently implanted, at 500 K with 3 keV helium ions to a dose of 5×10^{15} He/cm^2 using an ion gun mounted on a small turbo pumped vacuum chamber that achieved a base pressure of $< 10^{-7}$ mbar. Although the ion beam was not mass filtered, consideration of the base and helium pressures in various parts of the gun indicates that less than 0.05% of the ion beam was elements other than helium. Implantation was carried out at a flux of 6×10^{13} ions/cm^2/sec (< 30 mW/cm^2) giving rise to negligible heating of the specimen. In the present work, both helium and argon irradiations were carried out at 500 K. However, after transfer of the specimen into the HVEM, a 15 min anneal

was carried out at 670 K to grow the majority of the helium bubbles to a sufficient diameter (>3 nm) to render them visible. This growth was the result of thermal diffusion and coalescence of smaller bubbles.

Ar irradiations and *in situ* observations were performed at the HVEM-Accelerator Facility located at Argonne National Laboratory.[11] This facility consists of a modified Kratos/AEI EM7 high voltage electron microscope (HVEM) and a 0.6 MV National Electrostatics ion accelerator. Specimens were irradiated with the ion beam $10°$ away from the surface normal using a flux of 1.7×10^{12} Ar/cm^2 sec. The highest temperature produced by beam heating during Ar irradiation was estimated to be less than $10°$C. The effect of the irradiation on specific areas of specimens was recorded using both photographic film and videotape although the latter was only useful for bubbles of diameter 10 nm or greater. Higher resolution TEM was carried out using a JEOL 3010 TEM operating at 300 keV at the University of Salford.

The argon ion energy was chosen so as to produce atomic displacements in the bubble-containing gold film while minimizing argon implantation. Calculations using the Monte Carlo program TRIM (Ref. 12) indicate that for the experimental conditions used (400 keV Ar ions incident at $10°$ from the surface normal of a 50 nm thick gold film) only approximately 2% of the incident argon ions should come to rest in the film. For the highest doses used in the present work this would result in a concentration of implanted argon of only ≈ 0.03 at. %.

RESULTS

Figure 1 shows a series of images taken of a specific area of a helium-implanted gold specimen as a function of increasing argon dose. Significant changes have taken place after each increase in the argon dose. Figure 2 shows the bubble size distributions after each irradiation step (but obtained from a larger area than illustrated in Fig. 1). The statistical information reveals that the trend with increasing argon fluence is for small bubbles to disappear and the total number of bubbles to decrease while the overall distribution shifts to larger sizes.

In addition to statistical information, *in situ* irradiation in the TEM allows the fate of individual bubbles to be followed as a function of Ar irradiation. To illustrate the processes involved in bubble evolution more clearly, Fig. 3 shows the changes that have occurred between Figs. 1(c) and 1(d) (dose step from 2.55×10^{15} Ar/cm^2 to 3.40×10^{15} Ar/cm^2 or a change of 8.5×10^{14} Ar/cm^2). In Fig. 3, the original bubble position is indicated by a solid outline of the bubble, and the direction and distance of motion are respectively given by the direction and length of the arrow emanating from the bubble center. Bubble motion is assumed to have occurred when a bubble of similar size is found on Fig. 1(d) within 10 nm of a bubble position on Fig. 1(c). Bubbles that have disappeared between Figs. 1(c) and 1(d) are shown as a dashed outline, and bubbles that have appeared are shown as crosshatched.

Figure 3 displays a number of different processes. These are briefly described below.

A. Bubble disappearance

As expected from changes in the bubble size distribution, many bubbles have disappeared. The contrast of a large bubble, recorded on videotape, vanished over a period of approximately 1.5 sec. This is thought to be due to the bubble arriving at the foil surface and being converted to a crater which subsequently slowly "heals" by surface diffusion over the observation period. Surface image forces may play a role in this process. For smaller bubbles, not close to the surface, the time for disappearance could not be measured. On the basis of the depth distribution of the implanted He and resultant bubbles and the rate of bubble migration, discussed below, few bubbles are expected to reach a specimen surface by migration. Most bubble disappearances thus are likely to be the result of bubble disintegration by a single cascade resulting in He resolution.

B. Bubble shrinkage

In areas such as those marked on Fig. 3 with an A, a single bubble has greatly decreased in size ($A1$) or has been converted to several smaller bubbles ($A2$). This type of event is rare and has not been recorded on videotape. Such events may be the result of bubble disappearance at the surface followed by new bubble formation or more likely bubble disruption due to a direct hit by a large cascade. Both events result in He resolution.
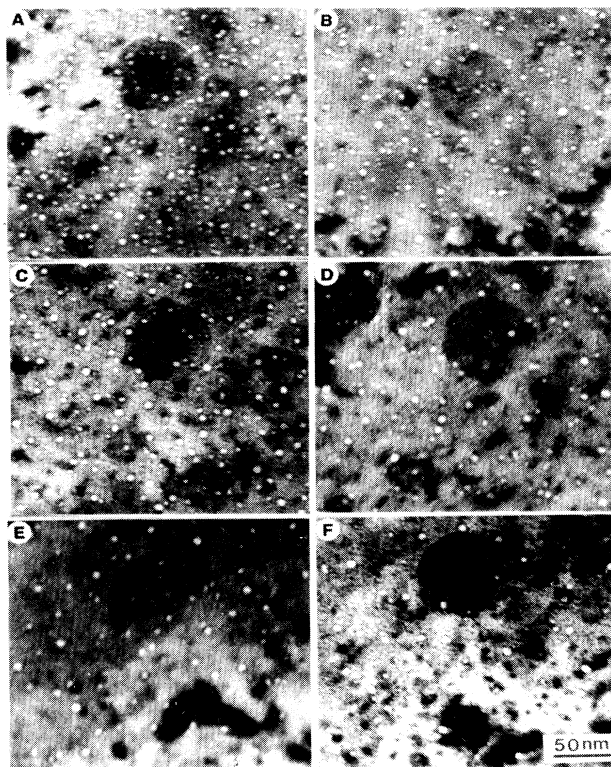

FIG. 1. Bright-field micrographs of helium bubbles in gold following irradiation with 400 keV Ar ions to fluences (ions/cm^2) of (a) 1.19×10^{15}, (b) 1.69×10^{15}, (c) 2.55×10^{15}, (d) 3.40×10^{15}, (e) 4.25×10^{15}, and (f) 5.0×10^{15}.
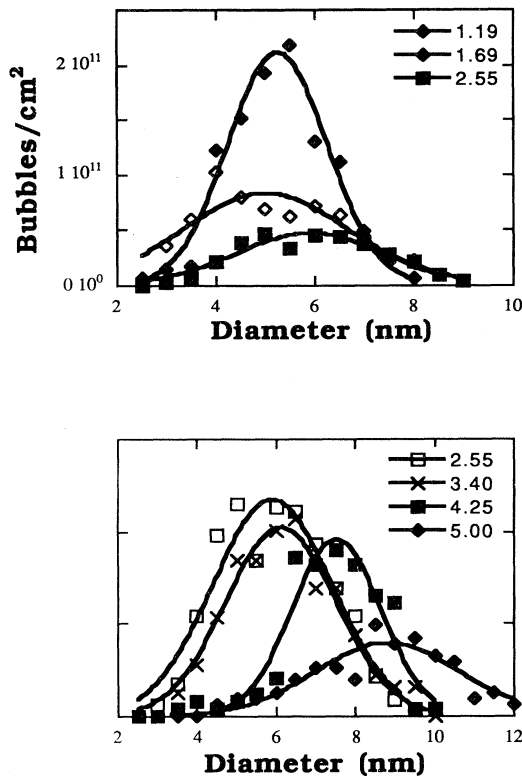
FIG. 2. He bubble size distributions after irradiation at 500 K with 400 keV Ar ions. The ion doses are the same as in Fig. 1 and are indicted on the figures in units of 10^{15} Ar/cm^2.

C. Bubble growth by coalescence

Many new bubbles are found in Fig. 3 at the site of two or more old bubbles. These are the remnants of bubble coalescence. Examples of the numerous coalescence events are marked B in Fig. 3. Bubble coalescence affects the bubble size distributions shown in Fig. 3 by removing

two or more small bubbles and shifting them to a single bubble at a larger size. In addition to the coalescence events observed between two visible bubbles, coalescence of submicroscopic helium vacancy clusters with visible bubbles presumably occurs. These events tend to offset He resolution noted above. Examination of a coalescence event between larger bubbles recorded on videotape shows that initially the new bubble is elongated but becomes more spherical during continued irradiation over a period of tens of minutes (doses of 10^{14} Ar/cm^2 to 10^{15} Ar/cm^2).

If bubbles are at equilibrium pressures, the sum of the square of the bubble's radii is a conserved quantity after coalescence.[10] The large amount of coalescence between dose steps in Fig. 1 prohibits following the development of an individual bubble, however, an average can be determined for the ensemble in Fig. 2. The sum of the individual bubble surface areas for all the visible bubbles measured in Fig. 2 will be referred to as the total bubble surface area. It is expressed in terms of bubble surface area for the number of bubbles in a unit area and is proportional to the fraction of the TEM image covered by bubbles. The total bubble surface area is shown as a function of Ar dose in Fig. 4. The total bubble surface area decreases during the early stages of the Ar irradiation and becomes constant above a dose of 2.5×10^{14} Ar/cm^2 or 0.6 dpa. Note that the failure to observe small bubbles leads to underestimation of the total bubble surface area at the lower doses. Loss of bubbles to the surface would cause a decrease in the value of the total bubble surface area. The rapid decrease in total bubble surface area with Ar irradiation indicates that the bubbles at 500 K were initially underpressurized. Recall that He implantation at 500 K was followed by an anneal to 670 K in order to grow the bubbles to larger more visible sizes. Cooling to 500 K reduced the bubble pressure leaving them underpressurized. The bubbles approach equilibrium at 500 K after coalescence during the initial part of the Ar irradiation.
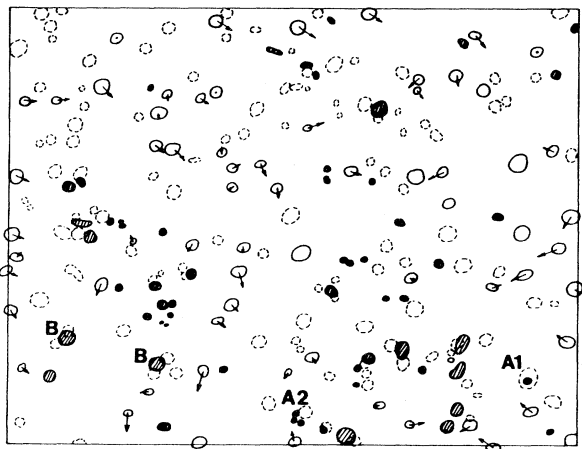

FIG. 3. Diagram of changes to bubbles occurring between Figs. 1(c) and 1(d). Arrow on bubble indicates direction and distance of motion. Dashed outline indicates that bubble has disappeared between Figs. 1(c) and 1(d). Diagonal hatching indicates that new bubble has appeared between Figs. 1(c) and 1(d).
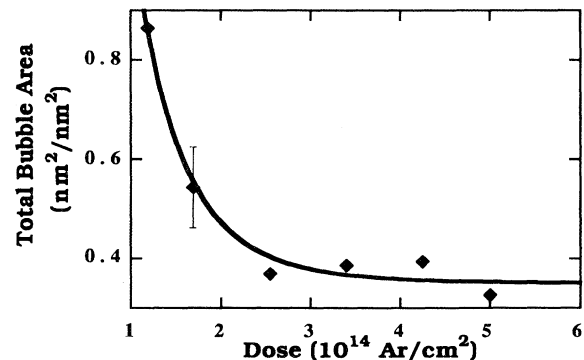

FIG. 4. Total surface area of observed He bubbles during irradiation at 500 K with 400 keV Ar ions expressed in terms of bubble surface area for the number of bubbles in a unit area. The ion doses are the same as in Figs. 1 and 2. The line is a guide to the eye.

D. Bubble motion

The most striking feature of Figs. 1 and 3 is the relative shift in bubble positions. The distance and direction of motion of those bubbles in Fig. 3 that survive the fourth dose step are shown in Fig. 5. (Note that the arbitrarily chosen X and Y directions are parallel with the horizontal and vertical axes of the images in Figs. 1 and 3.) There is stochastic bubble motion with a root-mean-square displacement per bubble on the order of 3 nm in both X and Y directions in the plane of the image (3.0 nm in X and 3.3 nm in Y) for this dose step of 8.5×10^{14} Ar/cm^2. It should be kept in mind that this figure does not include bubbles that disappear or coalesce. The small nonzero mean shift in position ($X \approx 0.7$ nm, $Y \approx -1.2$ nm) may be a result of either specimen bending or imprecise alignment between successive micrographs. Note that, based on Fig. 4, the He bubbles were at equilibrium pressures during measurement of their mobility.

TEM observations at 500 K without argon irradiation demonstrated that no change in the bubble distribution or position occurs over a time scale of hours, consistent with our annealing studies of He bubbles in Au.[13] Without irradiation, at 500 K the thermal vacancy concentration is 1×10^{-8} (Ref. 14) so that on average vacancies are separated by 20 nm. The changes observed in Fig. 5 are induced by the argon ion irradiation. Although Brownian motion of bubbles due to thermal diffusion has been previously observed at high temperatures,[15-18] this is the first direct observation of random bubble motion induced by any type of irradiation.

When helium bubbles in aluminum were irradiated at room temperature with 400 keV Xe ions, coalescence, shrinkage, and sputter-induced disappearance of bubbles were observed.[10] However, even for Xe doses of 1.5×10^{16} ions/cm^2, no bubble motion was detected. This is in marked contrast to the current work in which a significant degree of bubble movement is observed after each Ar dose.
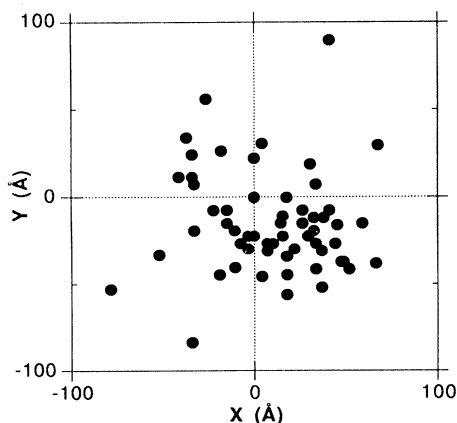

FIG. 5. Scatter plot of the motion of individual He bubbles occurring between Figs. 1(c) and 1(d). X and Y axes are parallel with horizontal and vertical axis of micrographs in Fig. 1.

DISCUSSION

Explanation for the diversity of processes observed in the present work can be found in the time evolution of the defect cascade (see review by English[19]). Four hundred keV Ar ions impinging on Au produce recoils with an energy distribution extending up to a maximum of 112 keV. Molecular dynamics simulations of atomic displacements in collision cascades in fcc metals support the model of a dense collision cascade first suggested by Brinkman.[20,21] Simulations by Diaz de la Rubia, Averback, and Hsieh[22] and Averback et al.[23] have shown that transfer of 5 keV to an atom in Cu or Ni results in a small liquidlike region with an effective temperature in the region in excess of 4000 K for times on the order of picoseconds. This "thermal spike" rapidly quenches at a rate dependent on the thermal properties of the metal. Because of self-interstitial atom transport away from the central melt zone by recoil collision sequences, the result is a vacancy rich, depleted zone.

Molecular dynamics simulation of cascades in Au have not been made, however, thermal spikes and melt zones are to be expected. Monte Carlo calculations performed using the TRIM computer code[12] reveal that a 400 keV Ar ion incident on a 50 nm gold layer at 10° to the surface normal (as in the present work) will yield an average of six subcascades each with a mean volume equivalent to a sphere having a diameter between 2 and 3 nm. TRIM calculations predict cascades with equivalent diameters as large as 10 nm.

Experimentally cascades in pure Au at room temperature collapse into dislocation loops and stacking-fault tetrahedra.[24-26] In materials containing dilute concentrations of He, this behavior is modified, and three-dimensional vacancy clusters are readily stabilized leading to void nucleation.[27] The high density of He bubbles mitigates these processes, and new bubble formation is associated with bubble destruction. An additional effect may occur when the collision cascade is initiated by an energetic ion penetrating through the specimen surface. Molecular dynamics simulations of 10 and 20 keV Au atoms impinging on a gold surface indicate that a surface cascade can crate a melt zone extending from the surface up to 7 nm in depth.[28] Material from such a depth may recoil back through the surface by viscous flow leaving a deep surface crater. The different processes observed in the experimental section are discussed below.

A. Bubble motion

The irradiation induced bubble motion can be analyzed in terms of cascade processes. Lacking any information on the atomic nature of the interaction of a cascade with a He bubble, we propose that a cascade initiated adjacently to a bubble will form a melt zone that will allow a bubble to deform into the molten region. Although we do not propose a precise mechanism, viscous flow processes may offer an explanation. The lattice disturbance involved with cascade collapse may play a role in such a process. We model bubble motion with the following simplifying assumptions: (i) bubbles and cascades are

spherical in shape, (ii) the spatial distribution of cascades through the gold foil is random and unaffected by the presence of bubbles, (iii) bubble-cascade interaction only occurs when a cascade volume touches or overlaps with a bubble, and (iv) the cascade thermal spike and localized melting results in the bubble moving to the center of the combined volume of the bubble and the cascade. For a given bubble, there is no preferential direction in which cascades will be created, and its motion will appear to be Brownian in nature.

The probability for a cascade to interact with a bubble is the product of the subcascade production rate and the interaction zone volume surrounding the bubble. The interaction rate is given by

$$N = \frac{4\pi}{3}[(r_b + r_c)^3 - r_b^3]n\varphi/t , \qquad (1)$$

where r_c is the cascade radius, r_b is the bubble radius, φ is the ion dose, n is the number of subcascades per ion, and t is the specimen thickness. For a separation between bubble and cascade centers of r_s, where $r_b < r_s \le (r_c + r_b)$, the distance moved by the bubble in the direction of the cascade, d, will be given by

$$d = r_s V_c / (V_b + V_c) , \qquad (2)$$

where V_c and V_b are the volumes of the cascade and bubble, respectively. This results in large bubbles moving a smaller distance than smaller bubbles. Since the probability, dP, of a cascade occurring in a given volume at given location relative to a bubble is proportional to the volume, the mean separation of centers of bubbles and cascades that do interact is given by

$$r_s = \frac{\int_{r_b}^{r_b + r_c} r \, dP}{\int_{r_b}^{r_b + r_c} dP} = \frac{3(r_b + r_c)^4 - r_b^4}{4(r_b + r_c)3 - r_b^3} . \qquad (3)$$

Note that the cascade is centered in the Au outside the He bubble and for a bubble much larger than the cascade, r_s approaches r_b leading to no motion.

For a random walk diffusion process, the rms distance moved is given by $d\sqrt{N}$ where d is the jump length and N is the number of jumps. For a bubble of diameter 5.5 nm [the mean value from Fig. 1(c)] interacting with cascades with mean diameters in the range 2–3 nm, Eqs. (1)–(3) yield values for the rms distance moved in the range 1.8 to 7.8 nm. This becomes 1.5 to 6.4 nm when projected onto the two-dimensional observational plane. The experimental value, obtained from Fig. 5, is 4.5 nm. This value is given by the above equations for a mean cascade diameter of 2.7 nm. The results of the calculations are sensitive to the value of cascade diameter so that a calculation averaging over cascade size distribution would be more appropriate. Nonetheless, given the simplicity of the model it is encouraging that bubble movement in agreement with experiment is calculated for a mean cascade diameter that is consistent with the results of both Monte Carlo and molecular dynamics calculations.

Since the process giving rise to bubble motion at low temperatures involves direct interaction between bubbles

and dense cascades, no such motion would be expected in low-Z materials where such cascades do not occur. Consistent with these expectations, no He bubble motion was observed in aluminum during heavy ion irradiation at room temperature.[10] Brownian bubble motion observed at high temperatures during *in situ* irradiation of Xe bubbles in Al with Al ions[29] and after irradiation of He bubbles in Fe 12 at. % Cr with Fe ions[30] was the result of bubble diffusion induced by freely migrating defects. Ion irradiation of He bubbles in alloys of Fe and 12 at. % Cr resulted in no bubble growth but a small degree of motion.[31] The difference between the experiments is that a true dense cascade is not formed in low-Z elements such as Al while it does form in higher-Z materials such as Au. The Fe alloys are an intermediate case.

B. Bubble disappearance and shrinkage

Many He bubbles disappear during irradiation. Because of the distances involved, bubble loss by motion to the foil surfaces fails to account for the experimental results. As has been found for other types of precipitates,[32] we presume that a He bubble would be strongly disrupted by an adjacent defect cascade. Molecular dynamic simulations of energetic cascades in many materials have shown that the initial stage of cascade development involves a substantial size melt zone.[22,23] A bubble incorporated into the melt zone of a large cascade could shrink (resolution) or disappear (disintegration) and possibly reform as several smaller bubbles. Disappearance may also result for viscous flow of a cascade zone toward the specimen surface.[28] Dense cascades do not form in lower-Z materials such as Al, and thus He bubbles in Al are not destroyed by a single cascade. Irradiation induced resolution of inert gas bubbles has been previously reported by Evans[9] for krypton in zirconium and by Birtcher, Donnelly, and Templier for He in Al,[10] but in both cases it was attributed to single gas atom recoils and not to the above mechanism.

Complete bubble destruction and resolution of He into mobile clusters allows both He loss from the specimen and gas driven bubble growth. Bubble movement during irradiation is also fairly high (~ 5 nm per 10^{15} Ar/cm^2). These processes can lead to significant loss of He by both atomic and bubble transport to surfaces and grain boundaries. In reactor fuels, these processes will make important contributions to steady-state release of fission gases.

C. Bubble coalesce and growth

Many He bubbles coalesce during irradiation. Bubble motion is one of several possible mechanisms. Immobile bubbles can also coalesce as a consequence of internal sputtering away of the material between two close bubbles.[10] A dense cascade in the region between two bubbles may produce melting and viscous flow allowing the bubbles to combine. The change towards a spherical shape that occurs in initially elongated bubbles formed by coalescence may be due to diffusion processes at the bubble surface enhanced by thermal spikes. Such irregularly shaped bubbles are far from equilibrium, and—provided that a suitable mechanism is available—are expected to

relax to a spherical shape. It is important to note that, except for coalescence events, individual bubbles do not grow. The lack of direct cascade driven growth is likely a consequence of the small number of freely migrating defects emitted from cascades[33] that could make changes to the number of vacancies in the bubble.

D. Bubble equilibrium

Variation of the total observed bubble surface area, Fig. 4, indicates that the bubbles were underpressurized after the 670 K anneal. The underpressure was relieved by bubble coalescence and growth after a dose of 2.5×10^{14} Ar/cm^2 or 0.6 displacements per atom. During the He implantation, a total of 0.05 dpa was produced in the Au of which a bubble, formed after some dose, would experience only a small part. The bubbles formed at 500 K may have been overpressurized, however, the bubbles approached thermal equilibrium for 670 K because of coalescence and growth during the anneal. Cooling to 500 K resulted in underpressurized bubbles at the start of the Ar irradiation. A consequence of this observation is that bubbles in moderate damaging environments will be at equilibrium pressures. This offers an explanation for observations after implantation, heavy inert gases in bubbles are at equilibrium pressures.[34]

CONCLUSIONS

We have studied the irradiation-driven evolution of He bubbles in the high-Z material Au. Under irradiation, bubbles were found to disappear, shrink, move, and coalesce. Bubble size evolution indicates that initially the annealed He bubbles were in an underpressurized condition, but Ar irradiation relieved the underpressure after a dose of 0.6 dpa. A consequence of this observation is that bubbles in even moderate damaging environments will be at equilibrium pressures. Comparison with similar experiments on He bubbles in a low-Z material, Al, demonstrates that dense defect cascades are responsible for both athermal bubble motion and bubble disintegration. Brownian bubble motion can be understood and modeled on the basis of bubble movement induced by the melt zone produced by the thermal spike of an adjacent dense cascade. Since dense cascades to not form in low-Z materials, He bubbles in Al are not subjected to these processes.

[1]*NATO Advanced Research Workshop on Fundamental Aspects of Inert Gases in Solids*, Vol. 279 of *NATO Advanced Study Institute, Series B: Physics*, edited by S. E Donnelly and J. H. Evans (Bonas, France, 1990).

[2]J. C. Rife, S. E. Donnelly, A. A. Lucas, J-M. Gilles, and J. J. Ritsko, Phys.Rev Lett. **46**, 1220 (1981).

[3]W. Jäger, R. Manzke, H. Trinkaus, R. Zeller, J. Fink, and G. Grecelius, Radiat. Eff. **78**, 315 (1983).

[4]P. B. Johnson and D. J. Mazey, Nature **276**, 595 (1978).

[5]J. H. Evans, A. van Veen, and L. M. Caspers, Nature **291**, 310 (1981).

[6]M. V. Speight, Nucl. Sci. Eng. **37**, 180 (1969).

[7]R. S. Nelson, J. Nucl. Mater. **31**, 153 (1969).

[8]J. A. Turnbull, Radiat. Eff. **57**, 243 (1980).

[9]J. H. Evans, *NATO Advances Research Workshop on Fundamental Aspects of Inert Gases in Solids* (Ref. 1), p. 307.

[10]R. C. Birtcher, S. E. Donnelly, and C. Templier, Phys. Rev. B **50**, 764 (1994).

[11]C. W. Allen, L. L. Funk, E. A. Ryan, and S. T. Ockers, Nucl. Instrum. Methods B **40/41**, 553 (1989).

[12]J. F. Ziegler, J. P. Biersack, and U. Littmark, *The Stopping and Ranges of Ions in Solids* (Pergamon, New York, 1985).

[13]J. H. Evans and A. van Veen, J. Nucl. Mater. **168**, 12 (1989).

[14]C. G. Wang, D. N. Seidman, and R. W. Balluffi, Phys. Rev. **169**, 553 (1968).

[15]L. E. Willertz and P. G. Shewmon, Metall. Trans. **1**, 2217 (1970).

[16]S. K. Tyler and P. J. Goodhew, J. Nucl. Mater. **92**, 201 (1980).

[17]L. J. Perryman and P. J. Goodhew, Act. Metall. **36**, 2685 (1988).

[18]J. H. Evans and A. van Veen, J. Nucl. Mater. **168**, 12 (1989).

[19]C. A. English, Radiat. Eff. **113**, 15 (1990).

[20]J. A. Brinkman, J. Appl. Phys. **25**, 8 (1954).

[21]J. A. Brinkman, Am. J. Phys. **24**, 246 (1956).

[22]T. Diaz de la Rubia, R. S. Averback, and. H. Hsieh, J. Mater. Res. **4**, 579 (1989).

[23]R. S. Averback, T. Diaz de la Rubia, H. Hsieh, and R. Benedek, Nucl. Instrum. Methods B **59/60**, 709 (1991).

[24]K. L. Merkle and W. Jäger, Philos. Mag. A **44**, 741 (1981).

[25]S. Ishino, N. Sekimura, K. Hirooka, and T. Muroga, J. Nucl. Mater. **141-143**, 776 (1986).

[26]W. Jäger and K. L. Merkle, Philos. Mag. A **57**, 479 (1988).

[27]I. Ishida, T. Yoshiie, S. Sasaki, A. Iwase, T. Iwata, and M. Kiritani, J. Nucl. Mater. **155-157**, 417 (1988).

[28]M. Ghaly and R. S. Averback, Phys. Rev. Lett. **72**, 364 (1994).

[29]D. E. Alexander and R. C. Birtcher, J. Nucl. Mater. **191-194**, 1289 (1992).

[30]P. Dauben, R. P. Wahi, and H. Wollenberger, J. Nucl. Mater. **141-143**, 723 (1986).

[31]Z. H. Lukinska and P. J. Goodhew, J. Nucl. Mater. **135**, 201 (1985).

[32]R. S. Nelson, J. A. Hudson, and D. J. Mazey, J. Nucl. Mater **44**, 318 (1972).

[33]L. E. Rehn and R. C. Birtcher, J. Nucl. Mater. **205**, 31 (1993).

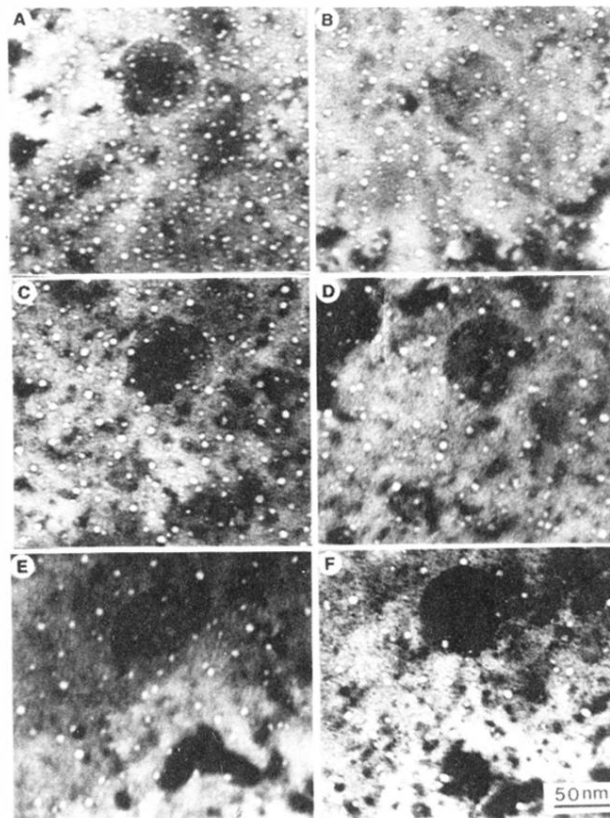[34]R. C. Birtcher and A. S. Liu, J. Nucl. Mater. **165**, 101 (189).

FIG. 1. Bright-field micrographs of helium bubbles in gold following irradiation with 400 keV Ar ions to fluences (ions/cm^2) of (a) 1.19×10^{15}, (b) 1.69×10^{15}, (c) 2.55×10^{15}, (d) 3.40×10^{15}, (e) 4.25×10^{15}, and (f) 5.0×10^{15}.